DOI 10.1007/s10946-016-9609-1
Journal of Russian Laser Research, Volume 37, Number 6, November, 2016

GENERALIZED CONCURRENCE AND NEGATIVITY IN TIME-DEPENDENT $C^3 \otimes C^5 = C^{15}$ DIMENSIONAL IONIC–PHONONIC SYSTEMS

Rasim Dermez

[1] *Department of Physics, Afyon Kocatepe University Afyonkarahisar 03200, Turkey*

[2] *Department of Electrical and Computer Engineering Michigan Technological University Houghton, Michigan 49931, USA*

[3] *Afyon Vocational School, Afyon Kocatepe University Afyonkarahisar 03200, Turkey*

*Author e-mail: dermez@aku.edu.tr

Abstract

We investigate the entanglement of a trapped three-level ion interacting with two vibrational phonons, which form a fifteen-dimensional Hilbert space. We reveal analytic formulas describing both the concurrence and negativity. We show that, in such a system, a higher degree of entanglement with a concurrence of 0.999 and a negativity of 0.499 can be attained at a specific time of 16.9 fs. Derived expressions of concurrence and negativity include first-order terms in the interaction picture. Finally, an explicit solution for first-order terms shows that the amount of concurrence can be tuned between 0 and 1.0, while the amount of negativity changes between 0 and 0.5.

Keywords: time-dependent Rabi frequency, time-dependent Lamb–Dicke parameter, concurrence, negativity, trapped three-level ion.

1. Introduction

As a direct consequence of the quantum entanglement, the philosophically comfortable tenets of local realism needs to abandoned [1, 2]. With the crucial role it plays in quantum optics and information, the emphasis on quantum entanglement has dramatically increased during the last thirty years. The fundamental question on quantum entanglement is: Which states are entangled and which ones are not? Trapped atomic ions are among the most attractive implementations of quantum bits for applications in quantum information processing, owing to their long coherence times [3, 4]. In particular, trapped atoms and ions are favored systems for studying and engineering quantum entanglement [5] due to their long decoherence times [6]. Experimental preparation of such profound and delicate nonclassical states are based upon sequential optical procedures [7].

There has been extensive research in the field of quantum communication, which has yielded a variety of methods to distribute bipartite entanglement [8, 9]. Quantum entanglement can be modeled physically by the states of a single and three-level trapped ions [10, 11]. Furthermore, entangled pure states can be produced by lasers and trapped three-level ions [12, 13]. Qudit entangled states in the second-order

Manuscript submitted by the author in English first on July 18, 2016 and in final form on August 27, 2016.

 1071-2836/16/3706-0572 ©2016 Springer Science+Business Media New York

corrections can help to answer some important questions about quantum linearity [14]. The three-different pure-state entanglement in the time-dependent ionic–phononic system have been demonstrated eventually [15].

On the theoretical side, we have worked out the quantum correlations of a full trapped ion interacting with two stationary laser beams [16]. We considered quantum dynamics of a three-level trapped ion using the quantum entropy of the system with time-dependent Rabi frequency [17]. In order to quantify quantum entanglement, the concurrence and negativity are uniquely determined by the spin–spin correlation between the impurities [18]. The entanglement entropy, which is an entanglement measure, is calculated in terms of the infinitesimal generator of conformal transforms that keep the sphere fixed [19]. Its relation to tomographic entropy associated to the spin-state tomograms was introduced in [20, 21]. In addition to these existing studies, in order to better identify long surviving states, we believe that the effects of the entanglement measurements in the quantum system are worthy of further inquiry.

Several Hamiltonian models are available, which describe the quantum entanglement of two-coupled atoms affecting by the time-dependent external magnetic field [22]. The inequality for eigenvalues of the density matrix and purity parameters describing either a bipartite-system state or a single-qudit state was studied in [23]. Similar to the correlations, analogous to the entanglement for the single qudit, they were formulated in terms of quantum contextuality [24]. A brief explanation of historical aspects of studying the properties of light and quantum correlations of photons and qudit states can be found in [25].

In this work, we develop a unitary transform method that is extended with respect to the weak excitation regime [26]. Our theoretical model possesses three crucial time-dependent parameters: Rabi frequency $\Omega(t)$, harmonic trap frequency $\nu(t)$, and Lamb–Dicke (LD) parameter $\eta(t)$.

This article is organized as follows.

In Sec. 2, we give the theoretical model as it is characterized in the weak excitation regime. In Sec. 3, we quantify the quantum entanglement of the time-dependent ionic–phononic system using concurrence and negativity. Finally, we give our conclusions in Sec. 4.

2. Theoretical Model of the Time-Dependent Ionic–Phononic System

Qubit logic gates can be implemented by engineering the quantum states and the interactions among these states [27]. This scheme bounds the center of mass vibrations within a region much smaller than the optical wavelength so that the coupling of the vibrational phonons to the internal states can be linearized. This is the so-called LD regime, which is described by a small LD parameter $\eta \ll 1$. Experiments operate beyond the LD regime where $\eta < 1$ [28, 29]. We assume that the lower levels of the three-level ion r and g are degenerate and the beams are of different polarizations so that each beam can drive only one transition. The time-dependent Rabi frequencies of the corresponding transitions $e - g$ and $e - r$, where e represents the excited level of the ion, are also considered to be the same and denoted by $\omega_1 = \omega_2$ (see Fig. 1).

In this paper, two time-dependent-amplitude laser beams are characterized by frequencies ω_1 and ω_2, where we assume $\omega = \omega_1 = \omega_2$. The time-dependent Rabi frequencies are $\Omega(t) = \Omega_1(t) = \Omega_2(t)$ assumed to be the same as in Fig. 1. The annihilation a and creation $a^\dagger$ operators of the vibrational phonons correspond to $a = \sqrt{\dfrac{m\nu(t)}{2\hbar}}\left(x + i\,\dfrac{p}{m\nu(t)}\right)$, where $\nu(t)$ is the time-dependent harmonic trap frequency, x is the direction along the trap axis, m is the mass of the ion, and p is the momentum of the center-of-mass of the ion.

The total Hamiltonian for the time-dependent ionic-phononic quantum system is

$$H(t) = H_{\rm ion}(t) + H_1(t) + H_2(t).$$

The Hamiltonian of the trapped ion $H_{\rm ion}(t)$ and the interacting Hamiltonians $H_1(t)$ and $H_2(t)$ at $\hbar = 1$ read

$$H_{\rm ion}(t) = \frac{p^2}{2m} + \frac{1}{2}m\nu^2(t)x_{\rm ion}^2 + \omega_{eg}|e\rangle\langle e|, \quad (1)$$

$$H_1(t) = \frac{\Omega_1(t)}{2}{\rm e}^{i(k_1 x_{\rm ion} - \omega_1 t)}|e\rangle\langle g| + {\rm h.c.}, \quad (2)$$

$$H_2(t) = \frac{\Omega_2(t)}{2}{\rm e}^{i(-k_2 x_{\rm ion} - \omega_2 t)}|e\rangle\langle r| + {\rm h.c.}, \quad (3)$$

where both wavelengths of the laser beams $\lambda = \lambda_1 = \lambda_2$ are slightly red detuned from the $e-g$ transition angular frequency of the ion ω_{eg} by the same amount $\delta = \nu(t)\eta^2(t)$, so that $\omega = \omega_{eg} - \delta$, with $\eta(t) = \dfrac{k}{\sqrt{2m\nu(t)}}$ being the time-dependent LD parameter and $k = \dfrac{2\pi}{\lambda}$. Additionally, the weak excitation regime is assumed to satisfy, $\nu(t) = \dfrac{\Omega(t)}{2}$.

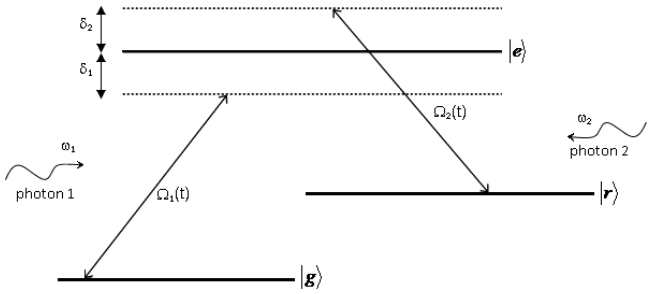

Fig. 1. Trapped three-level ion interacting with two time-dependent laser beams. The excited level e, the ground lever g, and the Raman level r are the intermediate and upper levels of the cascade, respectively. The other parameters are assumed to be $\Omega(t) = \Omega_1(t) = \Omega_2(t)$, $\omega = \omega_1 = \omega_2$, $\delta = \delta_1 = \delta_2$, $\omega_1 = \omega_{eg} - \delta_1$, and $\omega_2 = \omega_{eg} - \delta_2$.

We employ growing time-dependent Rabi frequency $\Omega(t) = \sinh(\omega_{eg}t)$ [30]. This rapid growth in time decreases $\eta(t)$, which eventually leads to the LD regime ($\eta(t) \ll 1$). Hence, our analytical results, which will be provided below, become almost precise, since we only use the correction to the first order in $\eta(t)$.

In the weak excitation regime, this Λ scheme has been shown to be equivalent to a cascade Ξ scheme for the vibrational phonon transitions, under a unitary transform, calculated by the transformation matrix U adopted from [26],

$$U = \frac{1}{2}\begin{pmatrix} 0 & \sqrt{2} & \sqrt{2} \\ -\sqrt{2}D[\eta(t)] & D[\eta(t)] & -D[\eta(t)] \\ \sqrt{2}D[-\eta(t)] & D[-\eta(t)] & -D[-\eta(t)] \end{pmatrix}, \quad (4)$$

where we represent the basis vectors as $\langle e| = (1,0,0)$, $\langle r| = (0,1,0)$, and $\langle g| = (0,0,1)$ and the Glauber displacement operators by $D(\eta) = \exp\left(i\eta(t)(a + a^\dagger)\right)$. Applying the unitary transform method of [26], we obtain the transformed Hamiltonian $\tilde{H}(t) = U^\dagger H(t) U$. This Hamiltonian describes cascade-type transitions of the vibrational phonons. Using Eq. (4) and the transformed Hamiltonian $\tilde{H}(t)$, we write the time evolution of the initial state $\psi(0)$ as follows:

$$|\psi(t)\rangle = U_0^\dagger U e^{-\int i\tilde{H}_0(t)dt} K(t) U^\dagger |\psi(0)\rangle, \quad (5)$$

where $K(t)$ is the well-known propagator for the cascade Hamiltonian [26], $\hbar = 1$, and $\exp[-\int i\,\tilde{H}_0(t)\,dt]$ are the interaction-picture transform. A given state of the vibrational phonons and the ion evolve in the Ξ configuration according to the propagator $K(t)$ in the interaction picture,

$$K(t) = \begin{pmatrix} \cos[\Lambda(t)t] & -\epsilon(t)S(t)a^\dagger & -\epsilon(t)S(t)a \\ \epsilon(t)aS(t) & 1+\epsilon^2(t)aL(t)a^\dagger & \epsilon^2(t)aL(t)a \\ \epsilon(t)a^\dagger S(t) & \epsilon^2(t)a^\dagger L(t)a^\dagger & 1+\epsilon^2(t)a^\dagger L(t)a \end{pmatrix}, \tag{6}$$

where $\Lambda(t) = \epsilon(t)\sqrt{2a^\dagger a + 1}$, $L(t) = \dfrac{\cos[\Lambda(t)t] - 1}{\Lambda^2(t)}$, and $S(t) = \dfrac{\sin[\Lambda(t)t]}{\Lambda(t)}$.

We take an ion in a harmonic trap with small vibrations, which can be considered as coherent displacements described by an approximately normalized coherent phononic state $|0\rangle + \alpha|1\rangle$ to the first order in α (i.e., $\alpha \ll 1$). We assume the superposition state $\dfrac{1}{\sqrt{2}}(|g\rangle - |r\rangle)$ so that the initial state for the ion–phononic system becomes

$$|\psi(0)\rangle = \frac{1}{\sqrt{2}}[(|g\rangle - |r\rangle) \otimes (|0\rangle + \alpha|1\rangle)]. \tag{7}$$

After action of the propagator $K(t)$ on the initial state of the cascade [i.e., $U^\dagger|\psi(0)\rangle$], we obtain the state $|\psi_K(t)\rangle = \sum\limits_{\mathrm{i}p} (M_{\mathrm{i}p}(t)\,|\mathrm{i}, p\rangle)$, where i stands for the electronic state (e, r, g) and p stands for the vibrational quantum number (0, 1, 2, 3, 4). The dimension of the Hilbert space $\mathbf{H} = \mathbf{H}_\mathrm{i} \otimes \mathbf{H}_p$ is 15. In the first-order terms, the probability amplitudes $M_{\mathrm{i}p}(t)$ are

$$M_{e0}(t) = \left[\cos\left[\sqrt{1/2}\,\nu(t)\eta(t)t\right] + \frac{i\eta(t)}{\sqrt{2}}\sin\left[\sqrt{1/2}\,\nu(t)\eta(t)t\right]\right] \mathrm{e}^{-i\nu(t)\eta(t)t}, \tag{8}$$

$$M_{e1}(t) = \alpha\cos\left[\sqrt{3/2}\,\nu(t)\eta(t)t\right]\mathrm{e}^{-i\nu(t)t}, \tag{9}$$

$$M_{e2}(t) = -\frac{i\eta}{\sqrt{5}}\sin\left[\sqrt{5/2}\,\nu(t)\eta(t)t\right]\mathrm{e}^{-2i\nu(t)t}, \tag{10}$$

$$M_{r0}(t) = \frac{\alpha}{\sqrt{3}}\sin\left[\sqrt{3/2}\,\nu(t)\eta(t)t\right]\mathrm{e}^{-i\nu(t)t}, \tag{11}$$

$$M_{r1}(t) = \frac{i\eta(t)}{\sqrt{2}}\left[(3/5) + (2/5)\cos\left[\sqrt{5/2}\,\nu(t)\eta(t)t\right]\right]\mathrm{e}^{-2i\nu(t)t}, \tag{12}$$

$$M_{g1}(t) = \left[\sin\left[\sqrt{1/2}\,\nu(t)\eta(t)t\right] - \frac{i\eta(t)}{\sqrt{2}}\cos\left(\sqrt{1/2}\,\nu(t)\eta(t)t\right)\right]\mathrm{e}^{-i\nu(t)\eta(t)t}, \tag{13}$$

$$M_{g2}(t) = \alpha\sqrt{2/3}\sin\left[\sqrt{3/2}\,\nu(t)\eta(t)t\right]\mathrm{e}^{-i\nu(t)t}, \tag{14}$$

$$M_{g3}(t) = -(\sqrt{3}/5)\,i\eta(t)\left[1 - \cos\left[\sqrt{5/2}\,\nu(t)\eta(t)t\right]\right]\mathrm{e}^{-2i\nu(t)t}, \tag{15}$$

and $M_{e3}(t) = M_{e4}(t) = M_{r2}(t) = M_{r3}(t) = M_{r4}(t) = M_{g0}(t) = M_{g4}(t) = 0$.

In the interaction picture, the final state can be written as follows:

$$|\psi(t)\rangle = \sum_{\mathrm{i}p} A_{\mathrm{i}p}(t)\,|\mathrm{i}, p\rangle, \tag{16}$$

where

$$A_{e0}(t) = 2^{-1/2}\,\mathrm{e}^{-i\omega t}\mathrm{e}^{-2iN(t)}M_{r0}(t), \tag{17}$$

$$A_{e1}(t) = 2^{-1/2}\,\mathrm{e}^{-i\omega t}\mathrm{e}^{-2iN(t)}M_{r1}(t), \tag{18}$$

$$A_{e2}(t) = 2^{-1/2}\,\mathrm{e}^{-i\omega t}\mathrm{e}^{iN(t)}M_{g2}(t), \tag{19}$$

$$A_{e3}(t) = 2^{-1/2}\,\mathrm{e}^{-i\omega t}\mathrm{e}^{2iN(t)}M_{g3}(t), \tag{20}$$

$$A_{e4}(t) = 2^{-1/2}\,\mathrm{e}^{-i\omega t}\mathrm{e}^{2iN(t)}M_{g2}(t), \tag{21}$$

$$A_{r0}(t) = i\sqrt{2}\,\eta(t)\mathrm{e}^{-iN(t)}M_{e1}(t) + \mathrm{e}^{-2iN(t)}M_{r0}(t) - i\eta(t)\mathrm{e}^{-2iN(t)}M_{r1}(t), \tag{22}$$

$$A_{r1}(t) = -\sqrt{2}\mathrm{e}^{-iN(t)}M_{e1}(t) + 2i\eta(t)\mathrm{e}^{-2iN(t)}M_{e2}(t) - i\eta(t)\mathrm{e}^{-2iN(t)}M_{r0}(t) + \mathrm{e}^{iN(t)}M_{g2}(t) + i\sqrt{3}\eta(t)\mathrm{e}^{2iN(t)}M_{g3}(t), \tag{23}$$

$$A_{r2}(t) = 2i\eta(t)\mathrm{e}^{-iN(t)}M_{e1}(t) - \sqrt{2}\mathrm{e}^{-2iN(t)}M_{e2}(t) - i\sqrt{2}\eta(t)\mathrm{e}^{-2iN(t)}M_{r1}(t) - \mathrm{e}^{-iN(t)}M_{g2}(t) + i\sqrt{3}\eta(t)\mathrm{e}^{iN(t)}M_{g3}(t), \tag{24}$$

$$A_{r3}(t) = i\sqrt{6}\eta(t)\mathrm{e}^{-2iN(t)}M_{e2}(t) + i\sqrt{3}\eta(t)\mathrm{e}^{iN(t)}M_{g2}(t) - \mathrm{e}^{2iN(t)}M_{g3}(t), \tag{25}$$

$$A_{r4}(t) = 2i\eta(t)\mathrm{e}^{2iN(t)}M_{g3}(t), \tag{26}$$

$$A_{g0}(t) = i\sqrt{2}\eta(t)\mathrm{e}^{-iN(t)}M_{e1}(t) + \mathrm{e}^{-2iN(t)}M_{r0}(t) + i\eta(t)\mathrm{e}^{-2iN(t)}M_{r1}(t), \tag{27}$$

$$A_{g1}(t) = \sqrt{2}\mathrm{e}^{-iN(t)}M_{e1}(t) + 2i\eta(t)\mathrm{e}^{-2iN(t)}M_{e2}(t) + i\eta(t)\mathrm{e}^{-2iN(t)}M_{r0}(t) + \mathrm{e}^{-2iN(t)}M_{r1}(t) - i\sqrt{2}\eta(t)\mathrm{e}^{iN(t)}M_{g2}(t), \tag{28}$$

$$A_{g2}(t) = 2i\eta(t)\mathrm{e}^{-iN(t)}M_{e1}(t) + \sqrt{2}\mathrm{e}^{-2iN(t)}M_{e2}(t) + i\sqrt{2}\eta(t)\mathrm{e}^{-2iN(t)}M_{r1}(t) - \mathrm{e}^{iN(t)}M_{g2}(t) - i\sqrt{3}\eta(t)\mathrm{e}^{2iN(t)}M_{g3}(t), \tag{29}$$

$$A_{g3}(t) = i\sqrt{6}\eta(t)\mathrm{e}^{-2iN(t)}M_{e2}(t) - i\sqrt{3}\eta(t)\mathrm{e}^{iN(t)}M_{g2}(t) - \mathrm{e}^{2iN(t)}M_{g3}(t), \tag{30}$$

$$A_{g4}(t) = -2i\eta(t)\mathrm{e}^{2iN(t)}M_{g3}(t), \tag{31}$$

and $N(t) = \int \nu(t)\,dt = \int \dfrac{\Omega(t)}{2}\,dt = \dfrac{\cosh(\omega_{eg}t)}{2\omega_{eg}}$. Here, there are 15 terms coming from the state in Eq. (16). Thus, we need the 15 probability amplitudes for the full density matrix ρ in order to calculate the concurrence and negativity in the next section.

3. Quantum Measurements: Concurrence and Negativity

Quantum entanglement is one of the cornerstones in quantum optics. The amount of entanglement in a quantum system is quantified by the well-known measures of entanglement called concurrence and negativity, which are what we employ in this paper as well. Hence, the quantum entanglement is characterized by comparing concurrence and negativity of the time-dependent ionic–phononic system. The internal states of the three-level ion subsystem are associated with a three-dimensional Hilbert space $\mathbf{H}_{\mathrm{i}}$ of a qutrit spanned by the basis states $\mathbf{H}_{\mathrm{i}}$, while the vibrational phonon subsystem is described by a five-dimensional Hilbert space $\mathbf{H}_p$. Therefore, the initial state in the previous section evolves in $3{\times}5$ ($C^3 \otimes C^5 = C^{15}$) dimensional Hilbert space. The density matrix of the system in a pure state $|\psi(t)\rangle$ is $\rho_{\mathrm{i}-p} = |\psi(t)\rangle\langle\psi(t)|$. In our case, $\rho_{\mathrm{i}-p}$ can be represented by a 15-dimensional matrix in the basis $|\mathrm{i}, p\rangle$. Concurrence for any arbitrary bipartite pure state is [31, 32]

$$C = \sqrt{2\big[\mathrm{Tr}\,(\rho_{\mathrm{i}-p}) - \mathrm{Tr}\,(\rho_{\mathrm{ion}}^2)\big]}. \tag{32}$$

In the time-dependent ionic–phononic system, the full density matrix $\rho_{\mathrm{i-p}}$ can be represented by a 15-dimensional square matrix in the basis of $|\mathrm{i}, p\rangle$. By tracing over the phononic variable, we obtain a 3×3-square reduced density matrix ρ_{ion} given by

$$\rho_{\mathrm{ion}} = \mathrm{Tr}_{\mathrm{phonon}}(\rho_{\mathrm{i}-p}) = \begin{pmatrix} \mathrm{Tr}|e\rangle\langle e| & \mathrm{Tr}|e\rangle\langle r| & \mathrm{Tr}|e\rangle\langle g| \\ \mathrm{Tr}|r\rangle\langle e| & \mathrm{Tr}|r\rangle\langle r| & \mathrm{Tr}|r\rangle\langle g| \\ \mathrm{Tr}|g\rangle\langle e| & \mathrm{Tr}g\rangle\langle r| & \mathrm{Tr}|g\rangle\langle g| \end{pmatrix}, \tag{33}$$

where $|e\rangle\langle e|$ is a 5×5 square matrix. In Eq. (33), the full density matrix $\rho_{\mathrm{i}-p}$ is written as

$$\rho_{\mathrm{i}-p} = \begin{pmatrix} |a\rangle\langle a| \end{pmatrix}, \tag{34}$$

where $|a\rangle\langle a|$ is a 15×15 square matrix and the basis vectors are $|a_1\rangle = |e, 0\rangle$, $|a_2\rangle = |e, 1\rangle$, $|a_3\rangle = |e, 2\rangle$, $|a_4\rangle = |e, 3\rangle$, $|a_5\rangle = |e, 4\rangle$, $|a_6\rangle = |r, 0\rangle$, $|a_7\rangle = |r, 1\rangle$, $|a_8\rangle = |r, 2\rangle$, $|a_9\rangle = |r, 3\rangle$, $|a_{10}\rangle = |r, 4\rangle$, $|a_{11}\rangle = |g, 0\rangle$, $|a_{12}\rangle = |g, 1\rangle$, $|a_{13}\rangle = |g, 2\rangle$, $|a_{14}\rangle = |g, 3\rangle$, and $|a_{15}\rangle = |g, 4\rangle$.

According to the Schmidt decomposition theorem, in order to study the negativity, we rewrite the pure state $|\psi\rangle$ as follows:

$$|\psi\rangle = \sum_j \sqrt{\mu_j}|a_j\rangle|b_j\rangle, \tag{35}$$

where $\sqrt{\mu_j}$ $(j = 1, \ldots, d)$ are the Schmidt coefficients (SCs) obtained from the eigenvalues of the reduced density matrix ρ_{ion}, and $|a_j\rangle$ and $|b_j\rangle$ are the orthogonal basis in $\mathbf{H}_{\mathrm{i}}$ and $\mathbf{H}_p$, respectively. The negativity of any arbitrary bipartite pure state $|\psi\rangle$ is given by [33]

$$N(|\psi\rangle) = \frac{2}{d-1}\sum_{i<j}\sqrt{\mu_i}\sqrt{\mu_j} = \frac{2}{3-1}(\sqrt{\mu_1}\sqrt{\mu_2} + \sqrt{\mu_1}\sqrt{\mu_3} + \sqrt{\mu_2}\sqrt{\mu_3}), \tag{36}$$

with $d = \min(d_1 = 3, d_2 = 5)$.

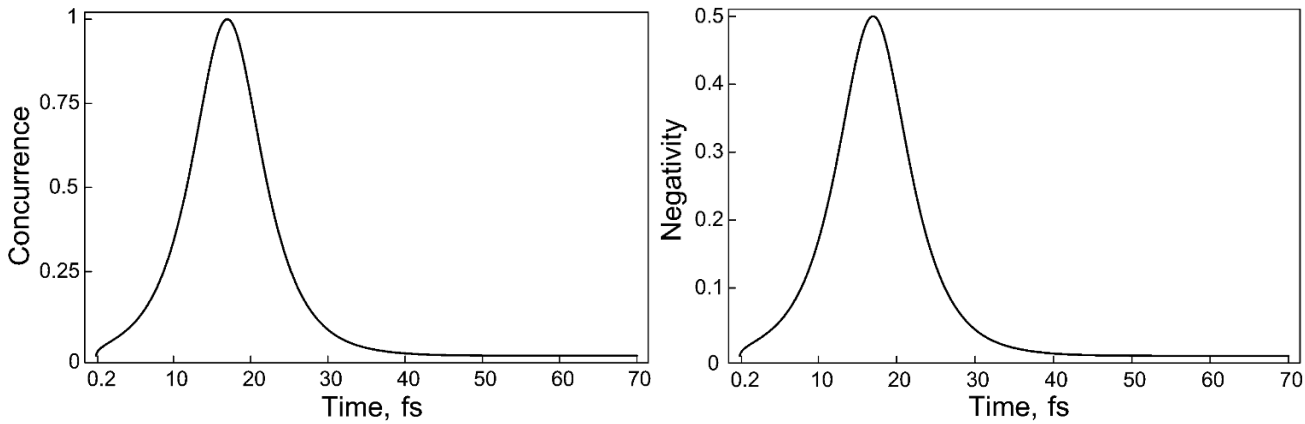

Fig. 2. The time evolution of the concurrence and negativity of the time-dependent ionic–phononic system in the 15-dimensional Hilbert space. The time-dependent harmonic trap frequency $\nu(t) = \dfrac{\sinh(\omega_{eg}t)}{2}$ and Rabi frequency $\Omega(t) = \sinh(\omega_{eg}t)$ are used with $\omega_{eg} = 5 \cdot 10^{14}$ Hz. The system is initially prepared in the state $\psi(0) = (1/\sqrt{2})(|g\rangle - |r\rangle) \otimes (|0\rangle + \alpha|1\rangle)$ with $\alpha = 0.01$.

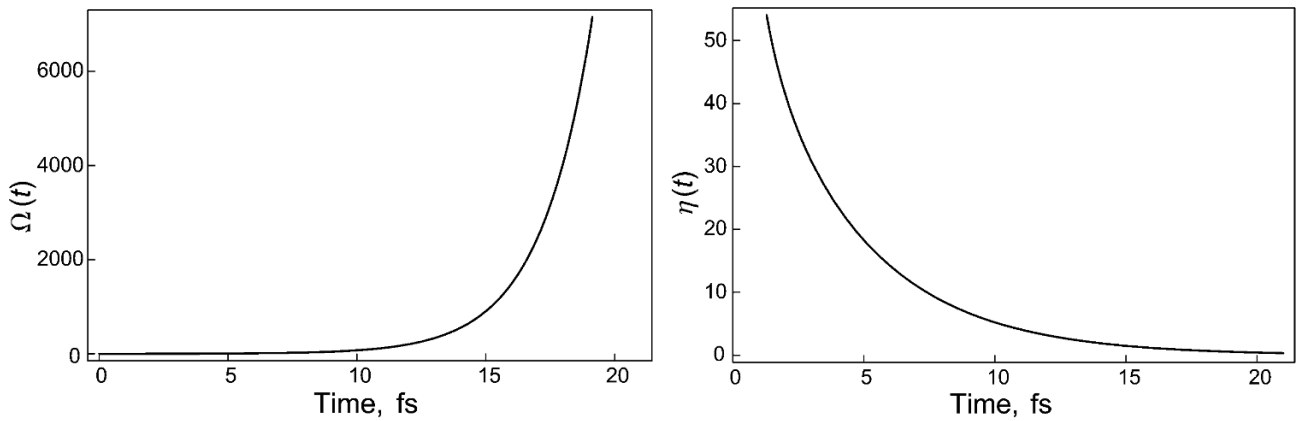

Fig. 3. The time dependence for $\Omega(t)$ and the scaled LD parameter $\eta(t)$ at $\hbar = 1$. The time-dependent ionic-phononic system is initially prepared in the state $\psi(0) = (1/\sqrt{2})(|g\rangle - |r\rangle) \otimes (|0\rangle + \alpha|1\rangle)$ with $\alpha = 0.01$ in the fifteen-dimensional Hilbert space.

In Fig. 2, we show two measurements of the quantum entanglement using Eqs. (32) and (36), where both curves resemble the Gaussian profile. In one of these plots, we elucidate the optimum entanglement of the system from $2.0 \cdot 10^{-16}$ to $7.0 \cdot 10^{-14}$ across time. We prepare Table 1 using the optimum entanglement of the time-dependent ion–phonon system of Fig. 2. We can compare negativity with concurrence in Table 1. We arrive at the same conclusions if we use negativity and concurrence as the entanglement measurements – the entanglement measurements then ensure the scale between $0-0.999$ (for concurrence) and $0 - 0.499$ (for negativity). We focus specifically on the effect of time-dependent Rabi frequency $\Omega(t)$ and time-dependent LD parameter $\eta(t)$. In Fig. 3, we illustrate the analytic evaluations of the entanglement measurements for $\Omega(t)$ (left panel) and $\eta(t)$ (right panel) for the optimum entanglement. The quantum entanglement values presented here are consistent with the quantum entropy studied in [17]. Moreover, these graphical observations are in accordance with that of mixed-state entanglement of [34].

Table 1. Values of C and N of Optimum Entangled Points for Fig. 2.[a]

Figure 2	$1 \cdot 10^{-14}$ s	$1.4 \cdot 10^{-14}$ s	$1.6 \cdot 10^{-14}$ s	$1.69 \cdot 10^{-14}$ s	$1.9 \cdot 10^{-14}$ s	$2.1 \cdot 10^{-14}$ s
Concurrence C	0.339	0.775	0.971	0.999	0.884	0.645
Negativity N	0.169	0.387	0.485	0.499	0.442	0.322

[a]The other parameters are the same as in Fig. 2.

In the figures, we assume $\omega_{eg} = 5 \cdot 10^{14}$ Hz and $\alpha = 0.01$ [26]. In Fig. 2, we see that the quantum entanglement of the systems exhibit a Gaussian-like profile as a function of time, and the concurrence reaches about 0.999 at the peak (left panel). This state is an approximately maximum entangled state for $1.69 \cdot 10^{-14}$ s. At the peak, i.e., $t = 16.9$ fs, we obtain the entangled state,

$$|\psi(t = 16.9 \text{ fs})\rangle = (5.69 \cdot 10^{-17}|e\rangle + 0.41|r\rangle + 0.41|g\rangle) \otimes |0\rangle + (0.31|e\rangle + 0.44|r\rangle + 0.44|g\rangle) \otimes |1\rangle$$
$$+(8.04 \cdot 10^{-17}|e\rangle + 0.29|r\rangle + 0.29|g\rangle) \otimes |2\rangle + (0.0|e\rangle + 3.09 \cdot 10^{-12}|r\rangle + 3.09 \cdot 10^{-12}|g\rangle) \otimes |3\rangle$$
$$+(8.04 \cdot 10^{-17}|e\rangle + 0.0|r\rangle + 0.0|g\rangle) \otimes |4\rangle. \quad (37)$$

Afterwards, the degree of entanglement monotonically decreases until the system reaches a separable

state. For instance, the electronic and phononic states of the ion get completely disentangled at $t =$ 70 fs$= 7.0 \cdot 10^{-14}$ s at the end of the plot in Fig. 2, where the system reaches the separable state. These disentangled states are seen in both the left and right panels in Fig. 2. Hence, the quantum entanglement results shown in Fig. 2 become more accurate after 70 fs, and $\eta(t)$ approaches zero after 21 fs (see Fig. 3, right panel). The analytic results in Eqs. (17)–(31) almost exactly describe the quantum dynamics of the ionic–phononic system since only the first-order correction in $\eta(t)$ is taken into account in these equations; this is in contrast to the time-independent analytic solutions of [12, 13].

4. Conclusions

In this paper, we analyzed the quantum entanglement process as a result of the time-dependent interaction of a three-level trapped ion with two laser beams in the Λ scheme using a unitary transform. At the same time, we focus on determining the entanglement generated by the system using the concurrence and negativity. It is an extension of our previous time-independent results [12,26] to the time-dependent analytical form that become exact when the LD regime is reached. The predicted quantum entangled states can be experimentally achieved in the LD regime at least for a certain period of time.

It is worth noting that the amount of quantum entanglement is the highest degree of concurrence and negativity, with the maximum of entanglement being reached at 16.9 fs$= 1.69 \cdot 10^{-14}$ s (see Fig. 2). With the help of Fig. 2, we show in Table 2 six different times of the optimum entangled points of concurrence and negativity. In this context, the consequences in Fig. 2 and Table 1 are in accordance with the previous studies [17, 34].

Punch-line result. We plotted the time evolution of the concurrence and negativity of the time-dependent 15-dimensional ionic–phononic system. Highlighting the two among many results of this paper are: (1) the amount of concurrence and negativity of entanglement exhibit the highest degree $C = 0.999$ and $N = 0.499$; (2) Rabi frequency $\Omega(t)$, harmonic trap frequency $\nu(t)$, and LD parameter $\eta(t)$ are time-dependent in the ionic–phononic system. Entangled states as demonstrated through first-order corrections by time-dependent coupling parameters and optimum entanglement can be beneficial for researchers in quantum computation and quantum optics. We hope such a practical availability of entangled states can be helpful for the ongoing efforts in ion–phonon-based quantum information where a high degree of entanglement can be useful for practical quantum computation applications.

Acknowledgments

This work was supported by the Afyon Kocatepe University under the 07-FENED.09 Project. The author thanks T. Dermez, C. Bulutay, and S. K. Tellioglu for their patience and Prof. Dr. O. E. Mustecaplioglu and O. D. Güney for their inspired communications.

References

1. A. Einstein, B. Podolsky, and N. Rosen, *Phys. Rev.*, **47**, 777, (1935).
2. J. S. Bell, *Physics*, **1**, 195 (1964).
3. P. Maunz, S. O. Moehring, K. C. Youge, et al., *Nature*, **3**, 538 (2007).
4. M. Qing-Xia, M. Yang-Hong, and L. Zhou, *J. Phys. B. At. Mol. Opt. Phys.*, **40**, 3241 (2007).

5. C. A. Sackett, D. Kielpinski, B. E. King, et al., *Nature*, **400**, 256 (2000).
6. C. Roos, T. Zeiger, H. Rohde, et al., *Phys. Rev. Lett.*, **83**, 4713 (1999).
7. C. Monroe, D. M. Meekhof, B. E. King, and D. J. Wineland, *Science*, **272**, 1131 (1996).
8. G. Gour and B. C. Senders, *Phys. Rev. Lett.*, **93**, 260501 (2004).
9. G. Gour, *Phys. Rev. A*, **71**, 012318 (2005).
10. S. A. Khalek, *Phys. Scr.*, **80**, 045302 (2009).
11. Z.-J. Wang and F. Chen, *Chin. Phys. Lett.*, **24**, 1570 (2007).
12. R. Dermez and Ö. E. Müstecaplıoğlu, *Phys. Scr.*, **71**, 015304 (2009).
13. R. Dermez and S. Özen, *Eur. Phys. J. D.*, **57**, 431 (2010).
14. R. Dermez and S. Özen, *Phys. Scr.*, **85**, 055009 (2012).
15. R. Dermez and S. A. Khalek, *J. Russ. Laser Res.*, **32**, 287 (2011).
16. R. Dermez, S. A. Khalek, K. Kara, et al., *J. Russ. Laser Res.*, **33**, 42 (2012).
17. R. Dermez, B. Deveci, and D. Ö. Güney, *Eur. Phys. J. D.*, **67**, 120 (2013).
18. S. Y. Cho and R. H. McKenzie, *Phys. Rev. A*, **73**, 012109 (2009).
19. H. Casini and M. Huerta, *Phys. Lett. B*, **694**, 167 (2010).
20. V. I. Man'ko and O. V. Man'ko, *J. Exp. Theor. Phys.*, **85**, 430 (1997).
21. M. A. Man'ko, V. I. Man'ko, and R. V. Mendes, *J. Russ. Laser Res.*, **27**, 507 (2006).
22. M. S. Abdalla, E. M. Khalil, A. S. F. Obada, and S. Sanad, *J. Russ. Laser Res.*, **37**, 10 (2016).
23. V. I. Man'ko and L. A. Markovich, *J. Russ. Laser Res.* **37**, 133 (2016).
24. A. A. Klyachko, M. A. Can, S. Binicioglu, and A. S. Shumovsky, *Phys. Rev. Lett.*, **101**, 020403 (2008).
25. I. Ya. Doskoch and M. A. Man'ko, *J. Russ. Laser Res.*, **36**, 503 (2015).
26. Ö. E. Müstecaplıoğlu, *Phys. Rev. A*, **68**, 023811 (2003).
27. D. Bouwmeester, A. Zeilinger, and A. Ekert, *The Physics of Quantum Information*, Springer, Berlin (2000).
28. D. F. V. James, *Appl. Phys. B*, **66**, 181 (1998).
29. L. F. Wei, Y. Liu, and F. Nori, *Phys. Rev. A*, **70**, 063801 (2004).
30. M. Abdel-Aty, *Opt. Commun.*, **266**, 225 (2006).
31. W. K. Wooters, *Phys. Rev. Lett.*, **80**, 2245 (1998).
32. S. Hill and W. K. Wooteers, *Phys. Rev. Lett.*, **78**, 5022 (1997).
33. S. Lee, D. P. Chi, S. D. Oh, and J. Kim, *Phys. Rev. A*, **68**, 062304 (2003).
34. R. Dermez, *J. Russ. Laser Res.*, **34**, 103 (2013).